COLD CRUCIBLE MELTING OF MURATAITE-CONTAINING CERAMICS

S.V. STEFANOVSKY, O.I. KIRJANOVA, S.V. YUDINTSEV, O.A. KNYAZEV
SIA Radon, 7th Rostovskii per., 2/14, Moscow 119121 RUSSIA

ABSTRACT

Murataite-based ceramics is a new waste form suitable for actinide and corrosion products immobilization. Three samples of the murataite-containing ceramics were produced in a bench-scale cold crucible based plant (60 kW, 1.76 MHz) and examined with X-ray diffraction, scanning and transmission electron microscopy. One of the samples with composition (in wt.%): 5.0 Al_2O_3, 10.0 CaO, 55.0 TiO_2, 10.0 MnO, 5.0 Fe_2O_3, 5.0 ZrO_2, and 10.0 UO_2 (actinides surrogate) is composed of major murataite and minor rutile and crichtonite. Additions of Gd_2O_3 (neutron absorber) and CeO_2 (PuO_2 surrogate) change the phase composition, forming pyrochlore-structured phase as major phase, murataite as second in abundance phase, and minor perovskite. The sample with the highest Ce content has the most complicated phase composition consisting of crichtonite as major phase, perovskite, zirconolite, rutile, murataite, and minor pseudobrookite. In the murataite-based sample two murataite varieties with five- and eight-fold fluorite cells have been found. Murataite grains appear zoned structure with maximum uranium concentration in the core. In the Gd and Ce containing samples only murataite with three-fold fluorite cell and relatively low U content has been observed.

INTRODUCTION

Murataite $A_4B_2C_7O_{20-22}$ is a new phase proposed for immobilization of actinide, rare earth and iron group elements [1-3]. Murataite ceramics are chemically durable [3] and may be suitable for immobilization of a long-lived zirconium-rare-earth – actinide (Zr-REE-An) fraction of high level waste (HLW) and excess weapons plutonium. It has been shown that murataite ceramics can be produced by both cold pressing and sintering and melting following by crystallization [1-5]. One of the most promising routes to crystalline waste forms is inductive melting in a cold crucible (IMCC) successfully applied earlier for production of various Synroc formulations [4,6-8], zirconolite [9-11], and pyrochlore-brannerite ceramics [8,12].

EXPERIMENTAL

The three formulations of the murataite containing ceramics (Table I) were designed, produced, and examined. Basic formulation (IMCC-1) was chosen to obtain a ceramic with maximum murataite content. Two other ceramic formulations contained gadolinium (IMCC-2) as neutron absorber and trivalent actinides and rare earths surrogate, and cerium (IMCC-3) as plutonium surrogate.

Table I. Specified formulations of the murataite ceramics (wt.%)

Samples	Al_2O_3	CaO	TiO_2	MnO	Fe_2O_3	ZrO_2	CeO_2	Gd_2O_3	UO_2	Crystalline phases
IMCC-1	5.0	10.0	55.0	10.0	5.0	5.0	-	-	10.0	M > R > C
IMCC-2	4.0	8.0	40.0	8.0	4.0	4.0	-	28.0	4.0	Py > M > P
IMCC-3	5.0	10.0	55.0	10.0	5.0	5.0	10.0	-	-	C > P > Z > R > M > Pb

C – crichtonite, M – murataite, P – perovskite, Pb – pseudobrookite, Py – pyrochlore, R – rutile, Z - zirconolite

Experiments were performed at a Radon bench-scale cold crucible unit (Figure 1) operated at 1.76 MHz with 60 kW vibration power. A cold crucible of 108 mm inside diameter manufactured from stainless steel pipes was placed within a copper inductor (number of coils – 4, inside diameter – 160 mm, height – 75 mm) coupled with a high frequency generator.

The cold crucible was filled with an oxide batch designed to obtain the ceramic with IMCC-1 formulation (Table I). Melting was initiated from a silicon carbide element capable of being heated in an AC high frequency electromagnetic field that was inserted in the batch. Experimental runs are shown in Table II.

Table II. IMCC runs.

Time from start, min.	Power, kW	Process run
IMCC-1		
0	20	Generator turning-on
2	33	Starting element heating, T ≈ 900 ^{0}C
5	33.6	Active gas release, melt formation
12	33	Starting element removal
17	38.5	Vibrating power increase
19	35	Melt temperature – 1550 ^{0}C
22	20	Batch feeding start. Selection of operation conditions and batch feeding rate
32	25	Batch feeding
37	20	End of batch feeding, holding for 5 min.
42		Melt pouring
IMCC-2		
0	36	Generator turning-on
2	36	Starting element heating, T ≈ 900 ^{0}C
6	36	Active gas release, melt formation
8	36	Starting element removal, batch feeding start
10	36	Batch feeding start. Selection of operation conditions and batch feeding rate
11	36	Batch feeding
12	30	Power reduction, batch feeding
13	30	Batch feeding, stable operation conditions
15	25	Power reduction
18	25	End of batch feeding, holding for 2 min. T ≈ 1500-1550 ^{0}C
20	20-22.5	Melt pouring
IMCC-3		
0	22.5	Generator turning-on
3	20.4	Starting element heating, T ≈ 900 ^{0}C
7	33.6	Active gas release, beginning of melt formation
8	33.6	Melt formation, T ≈ 1350 ^{0}C
15	25	Starting element removal, T ≈ 1450 ^{0}C, batch feeding start
25	35.7	T ≈ 1550 ^{0}C, melt has low viscosity
30	40	End of batch feeding, holding for 3 min.
33	35	Melt pouring

Fig. 1. The experimental unit.

Melt temperature was measured by an optical pyrometer. Introduction of Gd_2O_3 into the system reduces melting temperature as compared to the initial UO_2-bearing IMCC-1 melt. The melt with IMCC-3 formulation has the lowest viscosity and electric resistivity at 1500-1550 ^{0}C among the melts produced. The addition of Gd_2O_3 also stabilizes IMCC parameters, probably due to smoother variation of electric conductivity over operating temperature range. Murataite-containing ceramics may be easily produced by IMCC without significant overheating to reach suitable melt viscosity and resistivity.

Ceramic samples produced were examined with X-ray diffraction (XRD), optical microscopy (OM), scanning (SEM) and transmission electron microscopy (TEM) with energy dispersive spectroscopy(EDS) using a DRON-4 diffractometer (Cu K_α radiation), POLAM-L-213 microscope, JSM-5300 + Link ISIS unit, and a JEM-100c + KEVEX-5100 unit, respectively.

SAMPES EXAMINATION

XRD patterns of the samples studied are shown on Figure 2. Murataite was a major phase in Sample IMCC-1, accounting for about 75-80 vol.% of the sample. Rutile, crichtonite, and glass were minor phases. Their total amount in the sample did not exceed 20-25 vol.%. The sample (ingot) is composed of two zones,core and rim, The difference in size of grains depended on cooling rate. These parts have similar phase composition. Size of murataite grains in the rim is 20 μm and smaller whereas in the core they are larger – up to 40-60 μm. Regardless of their location, elements partitioning within the murataite grains in the sample show similar pattern in variation of elemental concentrations from rim to core of each grain. It is illustrated by data on enrichment (depletion) factors of rim with regard to core of the same grain (Table III). Its value is ratio of rim to core elemental concentrations (C_{rim}:C_{core}) within the murataite grains for the rim (K_{rim}) and the core (K_{core}) of the whole sample. As seen from Table III, K_{rim} and K_{core} values are close. This means uranium and zirconium contents reduce and manganese, aluminum, iron, and titanium contents increase as murataite grains grow.

Table III. Rim to core elemental concentrations ratio within the murataite grains.

Sample	K	Na	Al	Ca	Ti	Mn	Fe	Zr	Gd	U
IMCC-1	$K_{rim\ of\ sample}$	-	2.61	0.77	1.01	1.31	1.58	0.38	-	0.48
	$K_{core\ of\ sample}$	-	2.88	0.81	1.04	1.36	1.68	0.34	-	0.42
IMCC-2	$K_{rim} = K_{core}$	0.91	1.44	0.82	0.97	1.27	-	0.51	0.55	1.50

As follows from TEM data (Figure 3), Sample IMCC-1 contains at least two murataite varieties both with cubic fluorite-related lattice but differing in multiplicity of the fluorite unit cell. Murataites with five- (murataite-5x) and eight-fold (murataite-8x) fluorite cell have been found and one more murataite variety with three-fold fluorite unit cell (murataite-3x) may be also present. Formulae of the murataite in different parts of the grains from SEM/EDS data are given in Table IV. It can be suggested that murataite-5x forms core of the grains and murataite-8x composes rim. Occurrence of these varietiesappears on XRD patterns where two adjacent peaks due to different murataites are observed (Figure 2). One of them at 2.831 Å is probably due to murataite-5x and second one at 2.814 Å is due to murataite-8x. Because murataite-5x and murataite-8x compose the core and rim of the murataite grains respectively, the first one is formed at the early stage of melt crystallization whereas the second one is crystallized later from the melt with a different chemical composition. This may bethe reason why compositions of the core and the rim of the murataite grains are different.

Rutile crystals are 5-10 μm across. They have a tendency to form cross-like double intergrowths typical of rutile, which are connected in linear aggregates. Investigation of these aggregates in detail has shown that just their central parts (core) are composed of rutile while crichtonite forms the rim.

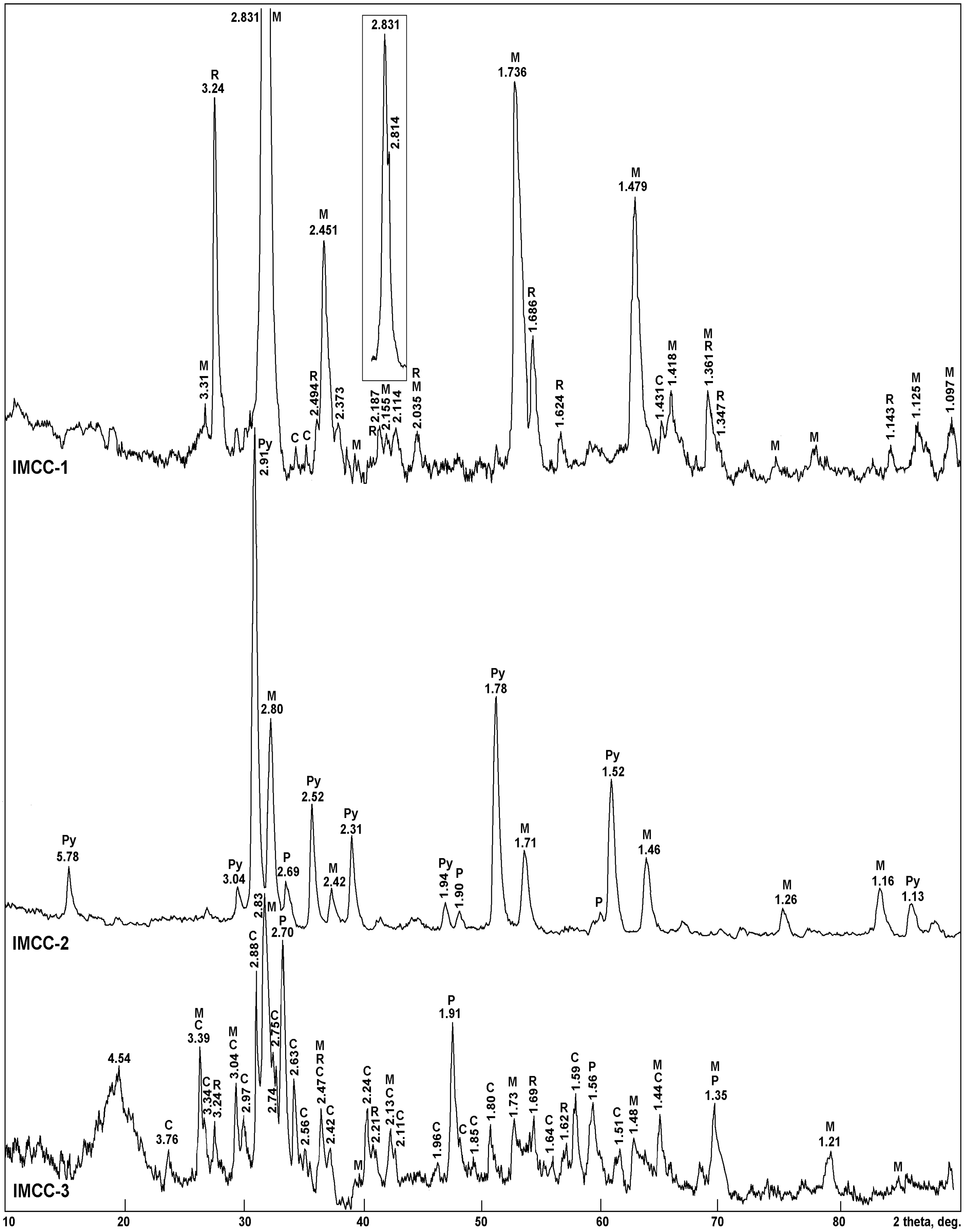

Fig.2. XRD patterns of the murataite-containing melted ceramics.

Symbols of the phases are the same as in Table I.

Crichtonite was also found as individual grains ~5 µm in size distributed within a glass. Rutile and crichtonite formulae are given in Table IV. The occurrence of interstitial glass is due to the dissolution of silicon carbide initiated melting of the batch and from a sodium-silica-based cold crucible protective putty. Chemical composition of this glass is given in Table V. Approximate amount of the phases in Sample IMCC-1 are (in vol.%): murataite – 75-80, rutile – 10-15, crichtonite – 5-10, glass – 1-4. The first phase crystallized from the melt is rutile following by formation of crichtonite and murataite.

Table IV. Formulae of the phases in the samples studied.

Phase	IMCC-1	IMCC-2	IMCC-3
Murataite-3x		$Na_{0.44}Ca_{1.21}Mn_{1.75}Gd_{0.52}U_{0.05}Ti_{5.64}Zr_{0.21}Al_{1.94}Fe_{1.23}O_{20.54}$	$Na_{0.31}Ca_{1.89}Mn_{1.28}Zr_{1.16}Ce_{0.16}Ti_{6.82}Al_{0.98}Fe_{0.41}O_{21.68}$
Murataite-5x (core)	$Ca_{2.15}U_{0.51}Zr_{0.61}Mn_{1.33}Ti_{6.95}Fe_{0.66}Al_{0.80}O_{21.80}$	-	-
Murataite-8x (rim)	$Ca_{1.64}U_{0.21}Zr_{0.19}Mn_{1.55}Ti_{6.49}Fe_{1.09}Al_{1.83}O_{21.35}$	-	-
Rutile	$Ti_{0.95}Zr_{0.03}Ca_{0.01}Al_{0.01}Fe_{0.01}O_{2.00}$	-	$Ti_{0.95}Zr_{0/04}Al_{0.01}O_{2.00}$
Crichtonite	$Ca_{1.45}U_{0.15}Zr_{0.13}Mn_{2.30}Ti_{13.95}Fe_{1.85}Al_{2.02}O_{38.00}$	-	$Ca_{1.03}Ce_{0.35}Zr_{0.73}Mn_{2.12}Ti_{13.93}Fe_{1.24}Al_{1.98}O_{38.00}$
Pyrochlore	-	$(Gd_{1.20}Ca_{0.29}Mn_{0.13}Zr_{0.19}U_{0.09})(Ti_{2.01}Al_{0.05}Fe_{0.04})O_{6.94}$	-
Perovskite-1	-	$(Na_{0.12}Ca_{0.55}Mn_{0.05}Gd_{0.23})(Ti_{0.92}Al_{0.05}Fe_{0.04})O_{3.00}$	$Na_{0.09}Ca_{0.64}Ce_{0.17}Mn_{0.02}Ti_{0.95}Al_{0.02}O_{3.00}$
Perovskite-2	-	$(Na_{0.12}Ca_{0.64}Mn_{0.05}Gd_{0.18})(Ti_{0.95}Al_{0.03}Fe_{0.03})O_{3.00}$	
Zirconolite	-	-	$Ca_{0.48}Mn_{0.45}Ce_{0.06}Zr_{0.72}Ti_{1.97}Fe_{0.15}Al_{0.24}O_{7.00}$
Pseudo-brookite	-	-	$Ti_{1.5}Mn_{1.0}Fe_{0.4}Al_{0.1}O_{5.0}$

Table V. Chemical composition (wt.%) of the vitreous phases in the samples studied.

Sample	Na_2O	Al_2O_3	SiO_2	CaO	TiO_2	MnO	Fe_2O_3	ZrO_2	CeO_2	Gd_2O_3	Total
IMCC-1	3.7	16.1	32.0	18.4	11.9	10.6	2.1	*	-	-	94.8
IMCC-2	5.7	20.2	35.6	12.2	8.7	12.4	3.8	*	-	1.4	100.0
IMCC-3	5.3	23.3	38.9	13.1	6.7	6.1	2.8	2.0	1.6	-	99.8

* lower than detection limit

Sample IMCC-2 is composed of major pyrochlore-structured rare earth titanate and minor murataite and perovskite as well as traces of vitreous phase (Table IV and Figures 2 and 3). Pyrochlore is found to be gadolinium titanate based solid solution (Table IV) accumulating 2-5 wt.% each of uranium, zirconium, calcium, and manganese. The phase second in abundance in this sample is murataite. A feature of its grain structure is the occurrence of a rim differing in chemical composition from the bulk of the grain. Elemental concentrations ratios in the core and in the rim are the same within experimental error. Thus, in the given case we observed the same elemental distribution patterns within single murataite grain as in Sample IMCC-1. The only difference is uranium behavior. In the murataite grains of Sample IMCC-1, uranium content in the rim is lower than in the core by more than a factor of two. For Sample IMCC-2, this difference is negligible (within the analytical error) and total formulation may be averaged as shown in Table IV. It should be noted that the composition of murataite in Sample IMCC-2 differs markedly from the murataite formulation in Sample IMCC-2. As follows from TEM data, this sample contains only the murataite-3x variety (Figure 3).

Minor phase perovskite is also present in Sample IMCC-2. Two types of perovskite grains were found (Table IV). One of them (perovskite-1) forms relatively large (20-50 µm) crystals of regular shape. The second variety (perovskite-2) forms regular grains smaller in size (usually 3-5 µm). They form aggregates of crystals confined in glass (Figure 3). Perovskites, especially perovskite-1, are enriched with gadolinium. These two perovskite varieties differ in calcium and, to a lesser extent, titanium, iron, and aluminum contents. This is probably due to the subsequent crystallization of the perovskite-2 from the melt depleted with gadolinium. The approximate phase composition of Sample IMCC-2 is (vol.%) pyrochlore –70, murataite – 20, perovskite – 10, glass - ~1. Mutual arrangement of the phases in Sample IMCC-2 points to their crystallization sequence as follows: pyrochlore – murataite + perovskite-1 – perovskite-2. The composition of residual glass is given in Table V.

Sample IMCC-3 is composed of major crichtonite (~50 vol.% of total) and perovskite (~30 vol.%), and minor zirconolite (~10 vol.%), rutile, murataite (~5 vol.% each), and traces of pseudobrookite (1-3 vol.%) and glass (≤ 1 vol.%) – see Figures 3 and 4. As in Sample IMCC-1, rutile grains are overgrown by crichtonite on their rim. Crichtonite forms the largest crystals (up to 50 µm) having an elongated or isometric shape dependent on cross section. The size of the grains of the rest of the phases does not exceed 20 µm. Perovskite and murataite grains have isometric shape. Perovskite grains form aggregates. Zirconolite forms prismatic crystals. Pseudobrookite was found in glass as thin needle-like crystals up to 20 µm in length and < 1 µm in width. Apparently, rutile is the first phase crystallized from the melt. The secondary phases segregated are crichtonite and zirconolite. Murataite and perovskite are the latest to be crystallized. Formulae of the phases in Sample IMCC-3 are given in Table IV. A feature of perovskite is high cerium content significantly exceeding its amount in the other phases. The glass composition is given in Table V. It is enriched with aluminum and silicon and depleted in manganese and titanium as compared to vitreous phases in the other samples.

DISCUSSION

The phase composition of the melted ceramics depends on waste elements composition and waste surrogate loading. Melted uranium and gadolinium containing ceramics have been established to have relatively simple phase assemblage and consist of three crystalline phases. Murataite is present in both the samples. In Sample IMCC-1 murataite predominates whereas in Sample IMCC-2 it is secondary phase being inferior in pyrochlore. Compositional variations affect structural features of murataite. In Sample IMCC-1 murataite varieties with five- and eight-fold fluorite unit cell have been found. While in Sample IMCC-2 only one murataite phase with three-fold fluorite cell has been observed. Sample IMCC-3 has the most complex phase assemblage being composed of six crystalline phases. Among them crichtonite is the predominate phase. This phase has relatively low capacity with respect to zirconium, rare earths, actinides, and iron group elements. This obviously is the reason why extra phases are capable of accommodating waste elements: perovskite for cerium, zirconolite for zirconium, murataite for manganese, aluminum, and iron are formed. Minor crichtonite phase with similar chemical composition was also present in Sample IMCC-1.

Formulae of the phases typical of ceramic waste forms and limiting contents of two groups of waste elements (Zr-REE-An fraction and corrosion products) are given in Table VI. Pyrochlore-structured titanate phase has maximum capacity with respect to actinides. However, its capacity with respect to corrosion products (iron group elements, Al) is very limited. A higher capacity with respect to these elements but some lower capacity with respect to rare earths and actinides is characteristic of zirconolite and murataite. In the whole (Table VI), murataite is the optimum phase from the point of view of simultaneous incorporation both Zr-REE-An fraction and corrosion products. Advantages of the murataite over the other host phases are lower actinide leaching at comparable radiation stability [13].

Table VI. Comparative characteristics of host phases with respect to various waste constituents

Phase	General crystal chemical formula	Maximal content, wt.%	
		Actinide fraction Zr+REE+An	Corrosion products (Al+Mn+Fe)
Pyrochlore	$A^{VIII}{}_2B^{VI}{}_2O_7$, A = Ca, Mn, REE, An; B = Ti, Zr	50	5
Zirconolite	$A^{VIII}B^{VII}C^{VI-IV}{}_2O_7$, A = Ca, Mn, REE, An; B = Zr, An, REE; C = Ti, Al, Fe	40	15
Perovskite	$A^{XII}B^{VI}O_3$, A = Na, Ca, REE, An; B = Ti, Al.	25	5
Murataite	$A_4B_2C_7O_{22-?}$, A = Ca, Mn, REE, An; B = Ti, Zr, C = Ti, Al, Mn, Fe	20	25
Crichtonite	$A_{1-2}{}^{XII}B^{VI-IV}{}_{19-21}O_{36-38}$, A = Ca, REE, An; B = Zr, Ti, Fe, Al	10	20
Oxide	$A^{VI}O_2$, A = Ti, Zr, U, Ca	5	1
Pseudobrookite	A_2BO_5, A = Mn, Fe, Al; B = Ti, Mn.	<1	40

CONCLUSIONS

Murataite-bearing titanate ceramics containing actinide waste surrogates were synthesized using the IMCC route at 1350-1550 ^{0}C. Melts of the ceramics studied have viscosity and electric resistivity values suitable for production of these ceramics at the temperatures indicated above. To immobilize waste with high actinide content murataite- and pyrochlore-based ceramics are preferable. Pyrochlore ceramics can accommodate high amount of actinide elements but low amount of corrosion products (Fe, Al, Mn). At high corrosion products content in waste, the murataite-based ceramics are more appropriate.

REFERENCES

1. S.V. STEFANOVSKY, S.V. YUDINTSEV, B.S. NIKONOV, B.I. OMELIANENKO, A.G. PTASHKIN, “Murataite-Based Ceramics for Actinide Waste Immobilization”, in Mat. Res. Soc. Symp. Proc. **556** (1999) 121.
2. N.P. LAVEROV, S.V. YUDINTSEV, B.I. OMELIANENKO, B.S. NIKONOV, S.V. STEFANOVSKY, “Murataite Ceramics for the Immobilization of Actinides”, in Geol. Ore Deposits **41** (1999) 85.
3. S.V. STEFANOVSKY, S.V. YUDINTSEV, B.S. NIKONOV, B.I. OMELIANENKO, “Phase and Chemical Stability of Murataite Containing Uranium, Plutonium, and Rare Earths” in 24th Symp. Sci. Basis for Nucl. Waste Manag. August 27 to 31, 2000. Sydney, Australia. Abstracts. P.4.1 (Mat. Res. Soc. Symp. Proc., 2001, to be published).

4. I.A. SOBOLEV, S.V. STEFANOVSKY, S.V. IOUDINTSEV, B.S. NIKONOV, B.I. OMELIANENKO, A.V. MOKHOV, "Study of Melted Synroc Doped with Simulated High-Level Waste", in Mat. Res. Soc. Symp. Proc. **465** (1997) 363.
5. I.A. SOBOLEV, S.V. STEFANOVSKY, B.F. MYASOEDOV, Y.M. KULIAKO, S.V. YUDINTSEV, "Phase Compositions of Murataite Ceramics for Excess Weapons Plutonium Immobilization", in Plutonium Future – The Science. Topical Conference on Plutonium and Actinides, Santa Fe, NM, USA, July 10-13, 2000. AIP Conf. Proc. 532 (2000) 148.
6. I.A. SOBOLEV, S.V. STEFANOVSKY, F.A. LIFANOV, "Synthetic Melted Rock-Type Wasteforms", in Mat. Res. Soc. Symp. Proc. **353** (1995) 833.
7. O.A. KNYAZEV, B.S. NIKONOV, B.I. OMELIANENKO, S.V. STEFANOVSKY, S.V. YUDINTSEV, R.A. DAY, E.R. VANCE, "Preparation and Characterization of Inductively-Melted Synroc", Proc. Int. Top. Meeting on Nuclear and Hazardous Waste Management SPECTRUM '96. Seattle, Aug. 18-23, 1996. ANS (1996) 2130.
8. S.V. STEFANOVSKY, O.A. KNYAZEV, D.B. LOPUKH, S.V. IOUDINTSEV, "The Cold Crucible Melting of Synroc", IT3 Conference. Int. Conf. On Incineration & Thermal Treatment Technologies. Proceedings. Salt Lake City, May 11-15, 1998. P. 155-158.
9. O.A. KNYAZEV, S.V. STEFANOVSKY, S.V. IOUDINTSEV, B.S. NIKONOV, B. I.OMELIANENKO, A.V. MOKHOV, A.I. YAKUSHEV, "Phase Equilibria and Elements Partitioning in Zirconolite-Rich Region of Ca-Zr-Ti-Al-Gd-Si-O System", in Mat. Res. Soc. Symp. Proc. **465** (1997) 401.
10. I.A. SOBOLEV, S.V. STEFANOVSKY, O.A. KNYAZEV, T.N. LASHTCHENOVA, V.I. VLASOV, D.B. LOPUKH, "Application of the Cold Crucible Melting for Production of Rock-Type Wasteforms", in Proc. Sixth Int. Conf. On Radioactive Waste Management and Environmental Remediation ICEM '97. Singapore, Oct. 12-16, 1997. ASME (1997) 265.
11. T. ADVOCAT, C. FILLET, J. MARILLET, G. LETURCQ, J.M. BOUBALS, A. BONNETIER, "Nd-Doped Zirconolite Ceramic and Glass Ceramic Synthesized by Melting and Controlled Cooling", in Mat. Res. Soc. Symp. Proc. 506 (1998) 55.
12. S.V. STEFANOVSKY, S.V. YUDINTSEV, B.S. NIKONOV, M.I. LAPINA, A.. ALOY, "Effect of synthesis conditions on phase composition of pyrochlore-brannerite ceramics", in Mat. Res. Soc. Symp. Proc. **605** (2000), in press.
13. S.V. YUDINTSEV, S.V. STEFANOVSKY, O.I. KIRJANOVA, J. LIAN, R.C. EWING, "Ion-Bombardment Induced Amorphization of Murataite in the Ceramic for Actinide Immobilization", in. Phys. Chem. Mat. Treat. 2001 (in press).